A1511

Model reduction approach applied to the thermal simulation of a solid oxide electrolysis stack

Quentin Brillaut (1,2), Christian Tantolin (2), Samuel Le Brozec (1), Manon Elie (2), Thomas Carlioz (2), Nicolas Massué (1), Patrice Tochon (1), F. Lefebvre-Joud (2)
(1) GENVIA SAS, Plaine Saint Pierre, 34500 Béziers/France;
(2) Univ. Grenoble Alpes – CEA/LITEN, 38054 Grenoble/France;
Tel.: +33438789743
quentin.brillaut@genvia.com

Abstract

The operation simulation of Solid Oxide Electrolysis Cell (SOEC) stacks requires multiphysics modelling approaches covering electrochemistry, mechanics, fluidics, thermal exchanges, etc. At component level, it can be done using CFD/FEM software packages [1], [2]. However, at system level where several stacks integrating many components are concerned, this kind of simulation is heavily time consuming.
In this perspective, we intend to simulate the thermal behavior of a stack within a SOEC system using a Reduced Order Model approach (ROM) based on the proper orthogonal decomposition methodology [3]. A Full Order Model (FOM) has first been developed to calculate a large number of operations cases and to constitute a learning cases database. Thanks to mathematical analysis, we have decreased the number of degrees of freedom and chosen to define subdomains, as homogeneous average media, in which thermal equations can be resolved. They reproduce the various parts of the stack having different and anisotropic thermal conductivity properties. As a first step, only the thermal transfer by conduction inside the stack has been considered as it is the predominant thermal phenomenon. Results from the ROM are compared to those from the FOM. The differences between the results of the two models, the impact of the selection of learning cases, the predictability of the ROM regarding real cases [4] and ultimately the calculation time are discussed.

Introduction

Numerical simulation of the operation of a solid oxide electrolysis cell (SOEC) stack requires a multi-physics approach covering the fields of electrochemistry, mechanics, fluidics, thermics etc. When the study concerns the analysis of one physics at a limited scale, CFD/FEM softwares appear fully suitable [1], [2]. However, when it addresses system scale, it becomes necessary to take into account all the physics involved and the use of those classical models becomes no more feasible due to very long calculation times.
In this context, our study focuses on the implementation of a model reduction methodology. Many ways can be considered: by reducing the size of the model, by simulating a 3D object in 2D, or by limiting the number of parameters taken into account. An interesting method, which we are considering in this work, consists in identifying the virtual axes carrying the most information, and in using them for the simulation. The Proper Orthogonal Decomposition (POD) is a widely-used reduction approach based on this principle [5], [6], [7].It has its roots in a statistical analysis developed at the beginning of the 20th century by Pearson [8]. Although improved, this approach remained limited by the computing power available at that time. In the 1960s, the approach was developed for fluid mechanics applications, such as turbulent flows [9], [10] or vortex flows [11], [12].
More recently, this reduction methodology with the POD approach has also been used for electrochemical and thermochemical systems. The electrochemical reactions taking place in batteries were simulated in 1D [13], [14]. Interestingly, heat transfers were added in [14] and the reduced model was used for real-time applications. The operation of a PEMFC cell in real time has also been reported [15]. Finally, in a thermochemical system for producing hydrogen by steam reforming of methane, a reduced model was developed, which enabled temperature sensors to be optimally positioned, and the complete thermal map of the system to be reconstructed [16]. To the best of the authors' knowledge, POD model reduction applied to water electrolysis systems, whatever the technology considered, in 3D, has not yet been reported.
The implementation of the POD approach consists in defining, from a set of experimental or numerical data, the axes of major variation on which to project the equations governing the system under study. In the work described below, these data sets are obtained by simulating the system's return to equilibrium from a defined initial state. Each simulation thus constitutes a scenario built from fixed operation parameters and covering significant durations. Each moment of this scenario constitutes a snapshot.
Below, we describe the construction of a physical model to simulate the thermal behavior of a SOEC stack, followed by the model reduction process and its validation.

1. Development of a Full Order Model (FOM)

In this work, we model the operation of an electrolysis stack. The stack is made up of 25 cells of 100 cm², surrounded by two end plates and two mechanical holding devices. The geometry of this system is broken down into 5 regions: (1) the ceramic multi-layer, (2) the gas inlet zone, (3) the sealing zone around the cell, (4) the end plate and (5) the mechanical holding device, Figure-1. These 5 regions are represented by equivalent homogeneous media with anisotropic properties (Table 1). This geometry is discretized into 7947 elements, 21 nodes along the x and y axes and 17 nodes along the z axis.

Table 1 : Properties of equivalent homogeneous media

Regions	$Cp\ (J.K^{-1}.kg^{-1})$	$\rho\ (kg.m^{-3})$	$\lambda_{xy}\ (W.m^{-1}.K^{-1})$	$\lambda_z\ (W.m^{-1}.K^{-1})$
Ceramic multi-layer	496.9	2384.9	10.8	1.4
Gas inlet zone	582.3	2384.9	11.9	1.06
Sealing zone	581.3	3559.4	10	0,38
End plate	660	11000	34.29	16.8
Mechanical holding device	660	7700	24	24

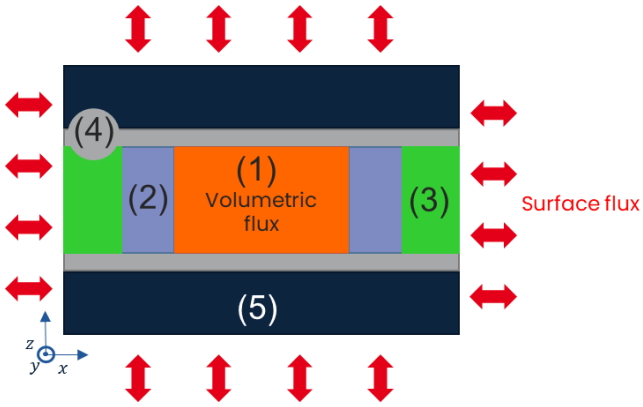

Figure-1 : Schematic of the stack broken down in 5 regions with average homogeneous properties (1) ceramic multi-layer, (2) gas entrance area, (3) sealing area surrounding the cell, (4) end plate and (5) mechanical holding device

In the present work, only heat exchanges by conduction, considered to be predominant, are taken into account. Convective heat exchanges within stack material are assumed to be negligible. However, heat source or heat sink effects linked to gas inlet temperatures are integrated in the thermal balance.
Consequently, the thermal behavior of the stack is assumed to follow the Fourier equation:

$$(\rho Cp)_{ijk}\frac{\partial T_{ijk}}{\partial t} = \frac{\partial^2(\lambda_{xy}T_{ijk})}{\partial x^2} + \frac{\partial^2(\lambda_{xy}T_{ijk})}{\partial y^2} + \frac{\partial^2(\lambda_z T_{ijk})}{\partial z^2} + q \qquad (1)$$

With $i, j\ and\ k$ the coordinates of the nodes along $x, y\ et\ z$, T_{ijk} the temperatures (K), ρ the density $(kg.m^{-3})$, Cp the thermal capacity $(J.K^{-1}.kg^{-1})$, λ_{xy} et λ_z the conductivities $(W.m^{-1}.K^{-1})$ and q $(W.m^{-3})$ combines the source terms and boundary conditions calculated by the equations given below.

The power of conduction thermal exchanges (P_{gas}) between the ceramic multilayer and gases is calculated with the following expression:

$$P_{gas} = \frac{\dot{m}_{Smix}Cp_{Smix}\left(T^{in}_{Smix} - T^{out}_{Smix}\right) + \dot{m}_{air}Cp_{air}\left(T^{in}_{air} - T^{out}_{air}\right)}{V_{ceram}} \qquad (2)$$

With P_{gas} the power $(W.m^{-3})$, $\dot{m}_{Smix}$ and $\dot{m}_{air}$ the mass flow rate $(kg.s^{-1})$ of $Smix$ (steam and hydrogen mixture) and of air, Cp_{Smix} and Cp_{air} the thermal capacities of the steam and hydrogen mixture and of air $(J.K^{-1}.kg^{-1})$, T^{in}_{Smix} and T^{in}_{air} the gas inlet temperatures (K) and T^{out}_{Smix} et T^{out}_{air} the gas outlet temperatures (K). These temperatures are taken to be equal to the temperature of the side surface of the ceramic multilayer. V_{ceram} is the volume of the ceramic multilayer (m^3).

In addition to heat exchange within the ceramic multilayer, the electrochemical reaction generates a thermal power given by the expression:

$$P_{electro} = \frac{(U - U_{TN}) * i * n_{cell} * S_{cell}}{V_{ceram}} \quad (3)$$

With $P_{electro}$ the power resulting from the electrochemical reaction, U the operation voltage of each cell (V), U_{TN} the thermoneutral voltage of each cell (V), i the current density of each cell ($A.cm^{-2}$), n_{cell} the number of cell in the ceramic multilayer and S_{cell} the surface of each cell (cm^2). Equations (2) and (3) are uniformly applied in the area of the ceramic multi-layer (Volumetric flux, Figure-1).

On the external faces, the radiative exchange between the stack and the furnace is calculated by the equation:

$$\varphi_j = -\sigma_0 E\left({T_{stack,j}}^4 - {T_{f,j}}^4\right) \quad (4)$$

With φ_j the power generated or absorbed ($W.m^{-2}$) by the surface j of the stack ($j = 1, \dots, 6$), σ_0 the Stefan-Boltzmann constant ($\sigma_0 = 5.67.10^{-8}\ W.m^{-2}.K^{-4}$), E the emissivity and $T_{stack,j}$ and $T_{f,j}$ the temperatures (K), of the surfaces j of the stack and j of the furnace facing each other. This power is calculated and applied uniformly over the entire surface j of the stack considered (Surface flux, Figure-1).

These equations are solved in the FOM model following a CFD/FEM resolution, and allow the thermal behavior of the stack to be simulated. An example of results is shown in Figure-2, in which the stack is subjected to 4 current density plateaus: 0.4, 0.8, 1.2 and 1.25 A/cm². These current density levels have been chosen to set the stack to endothermic (0.4, 0.8 A/cm²), thermo-neutral (1.2 A/cm²) and exothermic (1.25 A/cm²) conditions. The transition from one operating point to the next follows a ramp of 100s. Each operating step lasts 3000s.

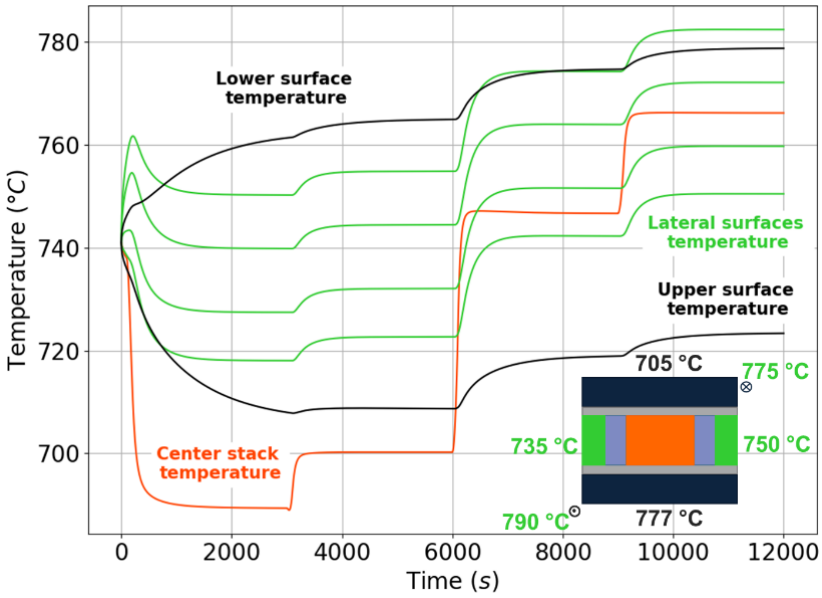

Figure-2: Results of the FOM: variation of stack temperatures, in the centre of the ceramic multilayer, on the side surfaces of the stack and on the top and bottom faces of the stack. The stack is subjected to 4 different current intensity plateaus during this simulation: 0.4, 0.8, 1.2, 1.25 A/cm²

Under the chosen flux and current conditions, the thermoneutral temperature is 750°C, so the first two operation conditions are endothermic, the third is thermoneutral and the last is exothermic. In the ceramic multilayer, both at the center and on the sides of the stack, temperatures initially stabilize below the initial temperature, confirming the endothermic nature of the operation. Between these two stabilization levels, a minimum temperature is reached, corresponding to the current density at which the endothermic nature of stack operation is at its maximum. As expected, the current level corresponding to thermo-neutral condition (1.2 A/cm²) is close to 750°C. The last intensity level brings the cell to a temperature higher than the initial temperature and the thermoneutral temperature. The top and bottom surfaces of the stack have both significantly different thermal behaviors compared to the other faces, due to the properties of the materials they are made of. As shown in Figure-2, the thermal interaction with the furnace predominates over the electrochemical power absorbed or released by the stack core. Thus, even in the endothermic regime, the lower face of the stack heats up to the temperature of the furnace, while in the exothermic regime the upper face of the stack remains at a temperature well below that of the thermo-neutral.

We also found that temperature stabilization times are longer on the bottom and top faces (>3000s) than on the side faces and ceramic multi-layer (<3000s), due to different thermal conduction properties of these regions.

This FOM, whose results were found to be rather faithful to the actual thermal behavior of a stack in operation, has been used to calculate various operation scenarios. Some of these scenarios have been used to build the matrix of training cases for the model reduction approach. Indeed, each time step of a learning scenario constitutes a learning case.

2. Development of a Reduced Order Model (ROM)

Methodology

The reduction method chosen is the POD, the mathematical principle presented here comes from [17], it allows the calculation of a matrix of size $N * M$ to be replaced by that of a matrix of smaller size.

The temperature matrix $\boldsymbol{\Theta}(\boldsymbol{x}, t)$ can be represented by a dataset $\overrightarrow{\theta(\boldsymbol{x}, t_i)}$, where $i = 1, \dots, M$ represents the index of time steps and $\boldsymbol{x}$ is the vector of x, y and z coordinates discretized on a spatial scale of $1, \dots, N$ with $N = Nx * Ny * Nz$. The vector $\overrightarrow{\theta(\boldsymbol{x}, t_i)}$ gives a thermal mapping of the stack at each instant t_i. The POD consists, from the M mappings of size N, in calculating an orthonormal basis in which the temperature field, at each instant t_i, can be written by the product of a diagonal matrix ($\boldsymbol{A}$) of singular values of size $min(N, M)$ and the spatial ($\boldsymbol{X}$) and temporal ($\boldsymbol{V^T}$) eigenvector matrices. We therefore try to write:

$$\boldsymbol{\Theta}(\boldsymbol{x}, t) = \mathbf{X} * \boldsymbol{A} * \boldsymbol{V^T} \quad (5)$$

With $\boldsymbol{\Theta}(\boldsymbol{x}, t)$ the temperature matrix, $\boldsymbol{X}$ the matrix of spatial eigenvectors, $\boldsymbol{A}$ the diagonal matrix of singular values and $\boldsymbol{V^T}$ the transpose matrix of temporal eigenvectors.

For each time t_i, this is equivalent to writing:

$$\overrightarrow{\theta(\boldsymbol{x}, t_i)} = \sum_{k=1}^{min(N,M)} \alpha_k(t_i)\overrightarrow{\chi_k}(\boldsymbol{x}) \quad (6)$$

With α_k the singular value scalar coefficients (resulting from the product $\boldsymbol{A} * \boldsymbol{V^T}$) and, $\overrightarrow{\chi_k}$ the orthogonal spatial eigenvectors.

To decompose the temperature matrix as described by equation (6) we need to look for the eigenvectors that maximize the product between $\vec{\theta}$ et $\vec{\chi}$. From the decomposition (Equations (5) and (6)), the model can be reduced. To do this, we take advantage of the specific properties of the $\boldsymbol{A}$ matrix, which returns the singular values in descending order. These values carry the weight of the associated eigenvector: the greater their value, the greater the variations along the associated eigenvector. So, in order to reduce the model, we can choose the n-first singular values that allow us to reproduce the thermal maps with an acceptable minimum level of error. To choose the number of eigenvectors to keep (K), a percentage criterion on their weight is proposed via the following relationship:

$$\frac{\sum_{k=1}^{n} \mathbf{A}_k}{\sum_{k=1}^{min(N,M)} \mathbf{A}_k} * 100 > \varepsilon \qquad (7)$$

With $\boldsymbol{A}_k$ the kth singular value and ε the criterion used, typically greater than 90%. The definition of this criterion is motivated by the aim of model reduction: to speed up the calculation while limiting the error generated by this reduction.

The temperature matrix can therefore be reconstructed using the reduced matrix product illustrated in Figure-3. The reduction using the POD approach allows the initial matrix calculation of size $N * M$ of the FOM to be replaced by a matrix calculation of size $K * M$. Note that an additional way of reducing the calculation time would be to reduce the number M of time nodes.

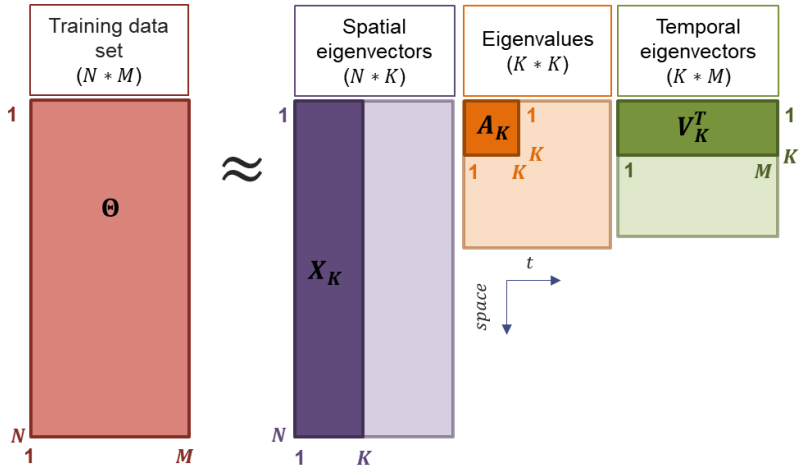

Figure-3: Selection of the k first couples singular values / eigenvectors

Learning cases choice

The construction of the matrix of learning cases is essential to define the axes of maximum variation and introducing spatial and temporal eigenvectors as well as singular values to reproduce the thermal maps of the stack as faithfully as possible. The aim is therefore to minimize the error between the results of the FOM model and those of the reduced ROM model. Various combinations of learning scenarios have been studied, and here we present a set of seven learning scenarios that give optimum results for the stack operating domain under consideration. A thermal condition is specified on each of the six faces of the stack. In this way, six learning scenarios are defined with balanced powers between the ceramic multilayer and one of the surfaces. One scenario with occasionally unbalanced starting conditions completes the set. These 7 scenarios are shown one after the other in Figure-4, as the values concatenated in the matrix of learning cases. A thermal map is selected every 10s to serve as a learning case.

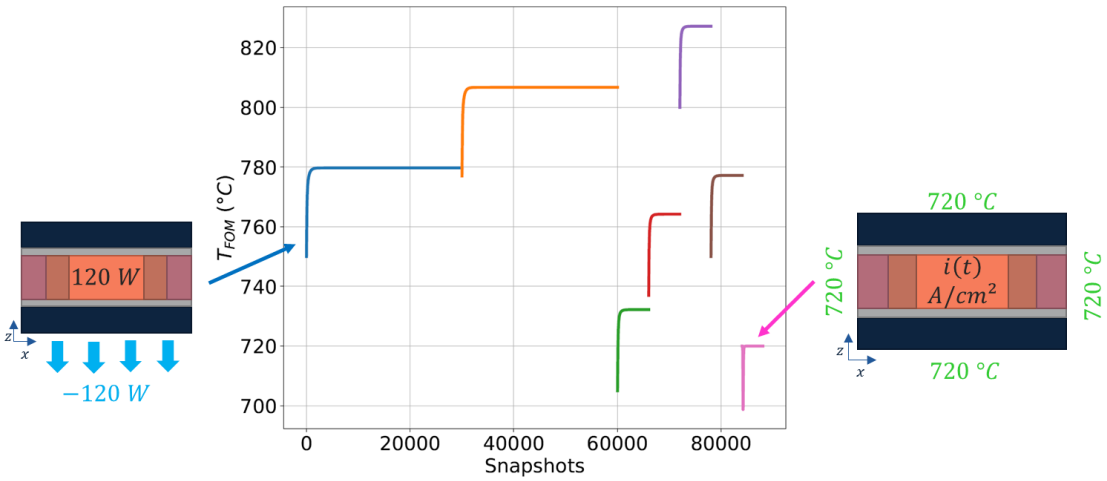

Figure-4: Temperature variations at the center of the stack for the 7 learning scenarios. The flow imposed on the lower surface is represented by the blue curve and on the upper surface by the orange curve. The green, red, purple and brown curves represent the temperature variations on the 4 lateral faces. The pink curve shows the case with punctually unbalanced boundaries conditions.

In each of the learning scenarios, the calculation is carried out until the temperatures have stabilized, which justifies the longer duration of the stabilisation stages in the first 2 scenarios. The initial temperatures are different for each case, in order to explore as wide an operating range as possible. A total of 8807 learning cases are taken into account in building the reduced model, so the learning matrix is 7497*8807 and induces 7497 eigenvectors. To select the number of eigenvectors onto which the equations will be projected, the criterion ε is set at 99.999%. As shown in Figure-5, this criterion is satisfied with the first 41 singular values, so the reduced model is constructed by projecting the heat conduction equation onto the 41 eigenvectors.

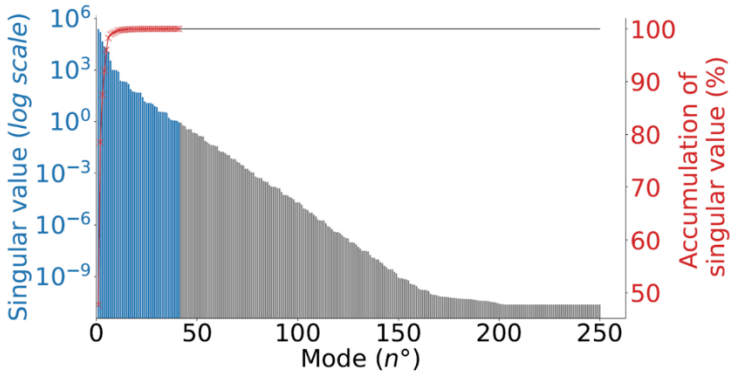

Figure-5: Values of the first 250 singular values in logarithm format (blue and grey bars). The red crosses and grey curve show the ratio of singular values selected to the total sum of singular values available. The blue bars and red crosses are the singular values selected by the chosen criterion value 99.999%.

3. Validation of the ROM by comparison with the FOM

Once the reduced model has been built, it needs to be validated. This validation is carried out by comparing the results obtained with the ROM model with those of the FOM model on one or more scenarios distinct from those used for training. In the case presented here,

corresponding to that shown in Figure-2**Erreur ! Source du renvoi introuvable.**, the comparison concerns the error between the results of the two models, FOM and ROM, and the respective calculation times. Figure-6 shows the temperature variations obtained with the FOM and ROM models. It can be seen that the average error between these two models is less than 0.01 K and that the maximum error is 0.06 K. The ROM model is therefore capable of simulating with a high degree of accuracy the thermal behavior of a SOEC stack under operating conditions that differ from the training scenarios.
The computation time of the ROM is 55 times faster than the FOM, enabling computation times compatible with its integration into a system model or its use in real time.

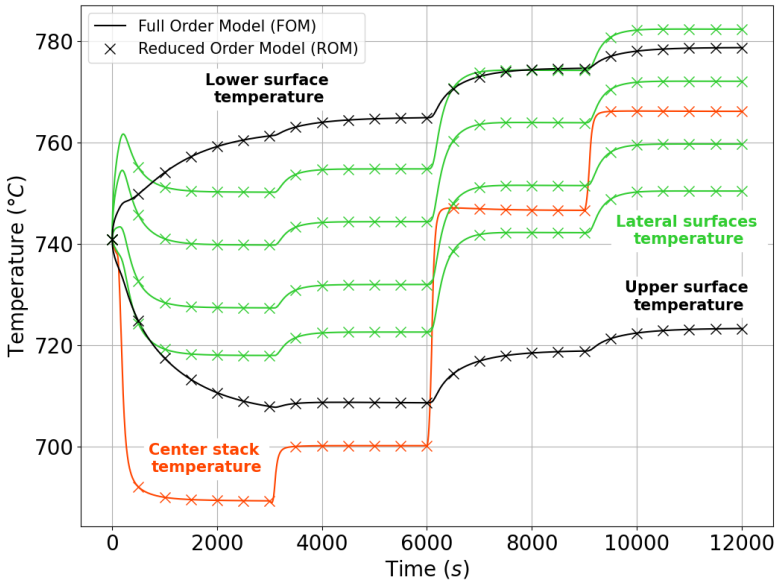

Figure-6: Temperature variation at 3 points on the stack: at the center of the cell stack, on the side surface of the stack and on the bottom surface of the stack. The stack is subjected to 4 different current intensity levels during this simulation: 0.4, 0.8, 1.2, 1.25 A/cm². The lines represent the variations of the reduced model, the crosses the variations of the complete model.

4. Conclusion

This study presents a model reduction methodology using a POD approach applied to a transient 3D model of the conductive thermal behavior of a SOEC stack. The performance of the reduced model constructed was compared with that of a complete physical model in terms of error and computation time. With a judicious choice of learning scenarios, the reduced model appears to reproduce satisfactorily the thermal behavior of the stack with a high degree of accuracy (less than 0.01 K) in the selected study domain, while dividing the calculation time by a factor of 55.
The continuation of this work will focus on comparing the results of this ROM model with experimental results, and on integrating a larger number of physical mechanisms.

References

[1] J. Udagawa, P. Aguiar, et N. P. Brandon, « Hydrogen production through steam electrolysis: Model-based dynamic behaviour of a cathode-supported intermediate temperature solid oxide electrolysis cell », *J. Power Sources*, vol. 180, nº 1, p. 46- 55, mai 2008, doi: 10.1016/j.jpowsour.2008.02.026.

[2] G. Delette *et al.*, « Thermo-elastic properties of SOFC/SOEC electrode materials determined from three-dimensional microstructural reconstructions », *Int. J. Hydrog. Energy*, vol. 38, nº 28, p. 12379- 12391, sept. 2013, doi: 10.1016/j.ijhydene.2013.07.027.
[3] F. Chinesta, R. Keunings, et A. Leygue, *The Proper Generalized Decomposition for Advanced Numerical Simulations*. in SpringerBriefs in Applied Sciences and Technology. Cham: Springer International Publishing, 2014. doi: 10.1007/978-3-319-02865-1.
[4] J. Aicart *et al.*, « Benchmark study of performances and durability between different stack technologies for high temperature electrolysis », *Fuel Cells*, 2023, doi: 10.1002/fuce.202300028.
[5] K. Karhunen, « Über lineare Methoden in der Wahrscheinlichkeitsrechnung », 1947.
[6] M. Loeve, « Functions aleatoires du second ordre », *Process. Stoch. Mouv. Brownien*, p. 366- 420, 1948.
[7] D. D. Kosambi, « Statistics in function space », *DD Kosambi Sel. Works Math. Stat.*, p. 115- 123, 2016.
[8] K. P. F.R.S, « LIII. On lines and planes of closest fit to systems of points in space », *Lond. Edinb. Dublin Philos. Mag. J. Sci.*, vol. 2, nº 11, p. 559- 572, 1901, doi: 10.1080/14786440109462720.
[9] A. A. Townsend, *The structure of turbulent shear flow*, 2. ed., Transferred to digital printing. in Cambridge monographs on mechanics and applied mathematics. Cambridge: Cambridge Univ. Pr, 1999.
[10] J. L. Lumley, « The structure of inhomogeneous turbulent flows. In Atmospheric Turbulence and Radio Wave Propagation », *Struct. Inhomogeneous Turbul. Flows*, p. 166- 178, 1967.
[11] L. Sirovich, « Turbulence and the dynamics of coherent structures. I. Coherent structures », *Q. Appl. Math.*, vol. 45, nº 3, p. 561- 571, 1987, doi: 10.1090/qam/910462.
[12] L. Sirovich, « Chaotic dynamics of coherent structures », *Phys. Nonlinear Phenom.*, vol. 37, nº 1- 3, p. 126- 145, juill. 1989, doi: 10.1016/0167-2789(89)90123-1.
[13] A. A. Shahbazi et V. Esfahanian, « Reduced-order modeling of lead-acid battery using cluster analysis and orthogonal cluster analysis method », *Int. J. Energy Res.*, vol. 43, nº 13, p. 6779- 6798, 2019, doi: 10.1002/er.4645.
[14] A. B. Ansari, V. Esfahanian, et F. Torabi, « Thermal-electrochemical simulation of lead-acid battery using reduced-order model based on proper orthogonal decomposition for real-time monitoring purposes », *J. Energy Storage*, vol. 44, p. 103491, déc. 2021, doi: 10.1016/j.est.2021.103491.
[15] A. B. Ansari, « Reduced-order modeling of PEM fuel cell based on POD and PODI: an efficient approach toward combining highest accuracy with real-time performance », *Int. J. Hydrog. Energy*, avr. 2023, doi: 10.1016/j.ijhydene.2023.04.096.
[16] B. Koo, T. Jo, et D. Lee, « Modified inferential POD/ML for data-driven inverse procedure of steam reformer for 5-kW HT-PEMFC », *Comput. Chem. Eng.*, vol. 121, p. 375- 387, févr. 2019, doi: 10.1016/j.compchemeng.2018.11.012.
[17] G. Berkooz, P. Holmes, et J. L. Lumley, « The Proper Orthogonal Decomposition in the Analysis of Turbulent Flows », *Annu. Rev. Fluid Mech.*, vol. 25, nº 1, p. 539- 575, janv. 1993, doi: 10.1146/annurev.fl.25.010193.002543.

Keywords: EFCF2024, Solid Oxide Technologies, SOC, Electrolysers, SOE, Stack modeling, Thermal Modeling, Model reduction methodology, Proper Orthogonal Decomposition